Neoplasia • Vol. 9, No. 1, January 2007, pp. 81–89 81

www.neoplasia.com

Telomere Attrition in Isolated High-Grade Prostatic Intraepithelial Neoplasia and Surrounding Stroma Is Predictive of Prostate Cancer[1]

Anthony Michael Joshua[*,†,‡], *Bisera Vukovic*[*,†], *Ilan Braude*[†,§], *Sundus Hussein*[¶], *Maria Zielenska*[§,#], *John Srigley*[¶,**], *Andrew Evans*[§,††] *and Jeremy Andrew Squire*[*,†,§,††]

*Department of Medical Biophysics, University of Toronto, Toronto, Canada; †Division of Applied Molecular Oncology, Ontario Cancer Institute, Princess Margaret Hospital, Toronto, Canada; ‡Department of Medical Oncology, Princess Margaret Hospital, Toronto, Canada; §Department of Laboratory Medicine and Pathobiology, University of Toronto, Toronto, Canada; ¶Department of Pathology, Credit Valley Hospital, Mississauga, Ontario, Canada; #Department of Pediatric Laboratory Medicine, The Hospital for Sick Children, Toronto, Ontario, Canada; **Department of Pathology and Molecular Medicine, McMaster University, Hamilton, Ontario, Canada; ††Department of Pathology, University Health Network, Toronto, Ontario, Canada

Abstract

The causes of early genomic events underlying the development of prostate cancer (CaP) remain unclear. The onset of chromosomal instability is likely to facilitate the formation of crucial genomic aberrations both in the precursor lesion high-grade prostatic intraepithelial neoplasia (HPIN) and in CaP. Instability generated by telomere attrition is one potential mechanism that could initiate chromosomal rearrangements. In this study, normalized telomere length variation was examined in a cohort of 68 men without CaP who had HPIN only on prostatic biopsies. Multiple significant associations between telomere attrition and eventual diagnosis of CaP in the HPIN and in the surrounding stroma were found. Kaplan-Meier analysis of telomere length demonstrated a significantly increased risk for the development of cancer with short telomeres in the surrounding stroma [*P* = .035; hazard ratio (HR) = 2.12; 95% confidence interval (95% CI) = 0.231–0.956], and a trend for HPIN itself (*P* = .126; HR = 1.72; 95% CI = 0.287–1.168). Cox regression analysis also demonstrated significance between the time from the original biopsy to the diagnosis of cancer and telomere length in HPIN and in the surrounding stroma. These analyses showed significance, both alone and in combination with baseline prostate-specific antigen, and lend support to the hypothesis that telomere attrition in prostatic preneoplasia may be fundamental to the generation of chromosomal instability and to the emergence of CaP.

Neoplasia (2007) **9,** 81–89

Keywords: Genomic rearrangements, DNA imaging, quantitative FISH, preneoplasia, telomere.

Introduction

Prostate cancer (CaP) is the most commonly diagnosed malignancy in men, with over a quarter of a million cases expected to be diagnosed in North America in 2006 [1,2]. However, an understanding of critical steps in the molecular and pathological etiologies of early prostatic carcinogenesis has not yet been achieved. Currently, the precursor lesion, high-grade prostatic intraepithelial neoplasia (HPIN), is considered the most likely preneoplastic precursor to CaP based on pathological [3], epidemiological [4,5], and molecular evidence [6]. The latter is especially suggestive of an association between the two lesions, with analyses of coexistent HPIN and CaP demonstrating similar chromosomal abnormalities, such as the characteristic loss of chromosome 8p and gain of chromosomes 8q, 7, 10q, and 16q, suggesting the emergence of chromosomal instability in HPIN [7]. Instability generated by telomere attrition in prostatic preneoplasia [8–10] is one mechanism that could facilitate the acquisition of consistent chromosomal rearrangements observed in HPIN [11,12].

Telomeres and associated nucleoprotein complexes are the terminal ends of eukaryotic chromosomes and contain up to

Abbreviations: CaP, prostate cancer; HPIN, high-grade prostatic intraepithelial neoplasia; H&E, hematoxylin and eosin; QFISH, quantitative fluorescence *in situ* hybridization; PNA, peptide nucleic acid; PSA, prostate-specific antigen

Address all correspondence to: Jeremy Squire, PhD, Ontario Cancer Institute, University Health Network, 610 University Avenue, Room 9-721, Toronto, Ontario, Canada M5G 2M9. E-mail: jeremy.squire@utoronto.ca

[1]This research was supported by a research training grant to the Princess Margaret Hospital/University Health Network from the Canadian Prostate Cancer Research Initiative; the University of Toronto Training program in Molecular Medicine; the Department of Defense Congressionally Directed Medical Research Program Predoctoral Traineeship Award (PC050531); and the Prostate Cancer Research Foundation of Canada.

Received 20 November 2006; Revised 19 December 2006; Accepted 20 December 2006.

Copyright © 2007 Neoplasia Press, Inc. All rights reserved 1522-8002/07/$25.00
DOI 10.1593/neo.06745

2000 repeats of the sequence TTAGGG [13]. Their primary role is to ensure chromosomal integrity by preventing the recognition of chromosome ends as DNA double-strand breaks, thus preventing recombination and leading to a cellular senescence response [14]. Telomere attrition and dysfunction may be due to several mechanisms such as the end-replication problem of chromosomal ends [15], which is believed to provide cells with a "mitotic clock" that limits cellular proliferation, thereby acting as a tumor-suppressor mechanism. However, continued cellular proliferation in the presence of shortened or dysfunctional telomeres results in end fusions and onset of chromosomal instability through break–fusion–bridge cycles [16]. Although these rearrangements are likely to lead to cell death, some surviving cells are thought to emerge, which eventually both stabilize their telomere lengths and control their level of instability through the reexpression of an enzyme called telomerase [17]. Telomerase adds telomeric sequence DNA to chromosomes and is expressed at varying levels in HPIN and at high levels in CaP [18–20]. The expression of telomerase and the acquisition of genomic alterations commonly observed in CaP, such as *TMPRSS2–ETS* fusion [21,22] and *PTEN* loss [12], are likely to be crucial to the subsequent progression of CaP from HPIN.

Up to 80% of CaP is both multifocal and associated with HPIN, suggesting a field effect of cancerization in the peripheral zone of the prostate, where these cancers are commonly found [23]. The molecular nature of this field effect is thought to involve only the prostatic epithelium. We reasoned that telomere length in the prostatic stroma may also be altered in the peripheral zone for two reasons. Firstly, etiologic agents involved in prostatic carcinogenesis may affect telomeres in the whole gland rather than in the epithelium only. Alternatively, it is conceivable that inheritance of shorter constitutional telomere length may itself be a risk factor for neoplastic progression in the prostate, as has been shown in other malignancies [24]. To explore these concepts, we examined normalized telomere length in a cohort of men who had isolated HPIN on prostatic biopsies with follow-up of up to 5.5 years. In this study, the amount of telomeric attrition in HPIN was accompanied by a proportional shortening in the surrounding stroma. We conclude that the extent of telomere attrition in such tissues may allow for improved prognostication of HPIN lesions into low or high risk for the development of eventual CaP, and may provide insights into the genomic mechanism of carcinogenesis in prostatic preneoplasia.

Materials and Methods

Tissue Accrual

Patient samples used in this study comprised a retrospective cohort derived from prostatic biopsies obtained through the UroPath Canadian Pathology Speciality Services over the period 1998 to 2000. The Research Ethics Board of the University Health Network (Toronto, Ontario, Canada) approved this study.

Description of Cohort

The characteristics of the cohort are described in Table 1. Men were biopsied using a sextant technique with six possible sites for biopsy. Seven of 34 (21%) men had the cancer diagnosed at the site of the HPIN biopsy available for the study; 12 of 34 (35%) had cancer diagnosed on the same side, whereas 19 of 34 (56%) had cancer diagnosed on the opposite side.

Pathology

Biopsy samples were formalin-fixed and paraffin-embedded. One biopsy per subject was analyzed. The biopsies usually consisted of a slither of tissue (approximately 1–2 mm by up to 15 mm). The initial cohort comprised 94 patients, all of whom had a recorded diagnosis of HPIN on the initial pathology review of prostatic biopsies. Following reevaluation of deeper sections by one of the authors (A.E.), a cohort of 68 patients who had evidence of HPIN and adequate stroma on deeper sectioning was identified for inclusion into this study. There were two to four deeper slides available from the original hematoxylin and eosin (H&E) slide used for HPIN identification, orientation, and further analyses. These regions and the surrounding areas of matching stroma were examined for telomeric and centromeric content using quantitative fluorescence *in situ* hybridization (QFISH). All investigators were blinded to patient outcome during the study period.

QFISH

QFISH was performed using pan-telomeric and pan-centromeric peptide nucleic acid (PNA) probes on unstained 5-μm sections. Telomere $(C_3TA_2)_3$–specific and centromere (16-mer α repeat DNA)–specific [25] probes were directly labeled with Cy3 and fluorescein isothiocyanate (FITC) fluorescent dyes, respectively, and were obtained from Applied Biosystems (Foster City, CA). The standard technique for PNA FISH [26] was applied with minor modifications, as described previously [8]. Slides were counterstained with DAPI/antifade (Vectashield, Burlingame, CA) and analyzed.

Image Capturing

Regions of interest were identified and marked on an overlying H&E section. Corresponding pathology was identified on FISH slides. The slides were analyzed with a Leica DMRA2 epifluorescence microscope (Leica Microsystems,

Table 1. Description of Study Cohort.

	Average	SD	Median	Range
PSA	8.8	6.95	8	0.7–51
Age	66 years	6.7	67	51–82
Time from first biopsy to final biopsy	18.82 months	16.52	14.5	1–69
Time to diagnosis of cancer (n = 34)	15.5 months	11.87	14	1–42
Number of biopsies until cancer was diagnosed (n = 34)	1.47	0.92	1	1–5
Gleason score (n = 34)	6.26	0.56	6	5–8

Wetzlar, Germany) equipped with appropriate filter sets, a mercury lamp, and a 100×/1.4-NA oil immersion lens. Twelve-bit grey-scale images were produced with a Hamatasu ORCA ER-17 camera (Hamatasu, Bridgewater, NJ) and OpenLab 4.0.3 software package (Improvision, Lexington, MA). To compensate for different focal depths, 10 consecutive images were z-stacked with an automated Leica CTRMIC interface (Leica Microsystems) into a composite image that was used for quantification. Images were saved and exported to the Image J software package [27]. Exposure times were optimized with respect to the intensities of telomere and centromere signals to prevent the overexposure/saturation of signals in the original and stacked images. Once optimization times had been determined, they were kept constant for all analysis experiments. Fluorescence output was verified to be within the linear range of assessment. An average of 50 cells from each HPIN and stroma on every slide was examined to quantify telomeric and centromeric signals with QFISH. Stromal cells were taken in random locations surrounding the HPIN gland identified for imaging. An optimal region for analysis was selected, avoiding areas of photobleaching and lipofuscin autofluorescence, typically within 1 mm of HPIN.

Image Assessment

Quantitative assessment of telomere/centromere signal intensity was performed on captured images and used to determine relative changes in telomere length and DNA ploidy. The original 12-bit images were exported to Image J. Initially, nonoverlapping nuclei were defined in a region-of-interest file. Subsequently, quantitative analysis was performed on a per-nuclear basis on Cy3 (telomere) and FITC (pan-centromere) images using visual thresholding to outline relevant signals [28]. The intensities of all pixels outlined within a predefined nuclear boundary were summed on a per-cell basis and tabulated. Absolute values for pan-centromeric QFISH indicate partial ploidy change, polysomies, hybridization differences, or amounts of nuclear material in a section. For example, theoretically, there will be a doubling of telomere signal per centromere as a result of every extra chromosome per HPIN cell. Thus, to control for ploidy and hybridization differences, all telomere intensities were expressed as telomeric intensity/centromere intensity ratios for each nucleus. These ratios were then averaged across the whole slide. An example of the approach taken in this study is illustrated in Figure 1.

Statistical Assessment

All statistical assessments were carried out with the "R" software package [29]. All correlations were examined with normalized telomere lengths. Statistical analyses for correlations for CaP outcome were carried out for significance using logistic regression and likelihood ratio tests. Standard *t*-tests were used to detect differences between mean telomere values of men who developed cancer and men who did not develop cancer. Cox regression modeling was used to determine the association of time to diagnosis with normalized telomere length, as well as the calculation of hazard ratios (HRs) and confidence intervals for Kaplan-Meier analysis. Standard Kaplan-Meier analysis was carried out to explore the time to diagnosis of cancer stratified by telomere length in HPIN.

Results

Fluorescence Variables

Absolute fluorescence values Total centromeric intensity in HPIN, compared to total centromeric intensity in the surrounding stroma, revealed an average increase of 22% in centromeric fluorescence (SD = 31%) (Figure 2*A*). In comparison, absolute telomeric intensity measured in HPIN divided by that in the surrounding stroma revealed that the telomeres in HPIN were, on average, 36% of those in the surrounding stroma (SD = 21%) (Figure 2*B*).

Normalized fluorescence values Inspection of normalized QFISH values alone for both HPIN and stroma did not reveal any population of uniform telomere length among cells (Figure 2, *C* and *D*). There did not appear to be any relationship between telomere length in HPIN or in the stroma and patient age on initial biopsy (adjusted $R^2 = 0.052$ and 0.104, respectively). Additionally, there was also no correlation between prostate-specific antigen (PSA) level and telomere length, suggesting that these may be independent phenomena (adjusted $R^2 = -0.007$ and 0.006, respectively). The most notable finding was the relationship found between the stroma and the epithelium. There appeared to be a significant association between the telomere length in the HPIN and that in the surrounding stroma (adjusted $R^2 = 0.4697$; $P = 1.14 \times 10^{-10}$) (Figure 4*A*).

Statistical Correlations

Analysis for CaP outcome As the cohort of men did not have time-mandated or event-mandated biopsies, we initially calculated logistic regression statistics for the diagnosis of CaP after particular time points had elapsed. The time variable corrects for men who were lost to follow-up after a negative biopsy subsequent to the time indicated in Table 2. Multivariate modeling at these time points, combining telomere length measurements and PSA, also showed high levels of significance (e.g., 3 months: PSA + HPIN, $P = .019$; PSA + stroma, $P = .015$). *P* values calculated for the association between telomere length and PSA by logistic and multivariate analyses are presented in Table 2. Alternatively, standard *t*-test analyses and accompanying boxplots for telomere length in both HPIN [*t*-test: $P = .03$; 95% confidence interval (95% CI) = 0.004–0.080] and stroma (*t*-test: $P = .04$; 95% CI = 0.004–0.188) with the final diagnoses are illustrated in Figure 3, *A* and *B*.

Cox regression modeling for time to diagnosis Cox regression modeling demonstrated that the telomere length of HPIN and of the surrounding stroma also predicted the time to diagnosis of cancer from initial biopsy, both alone ($P = .015$ and $P = .021$, respectively) and in combination with PSA

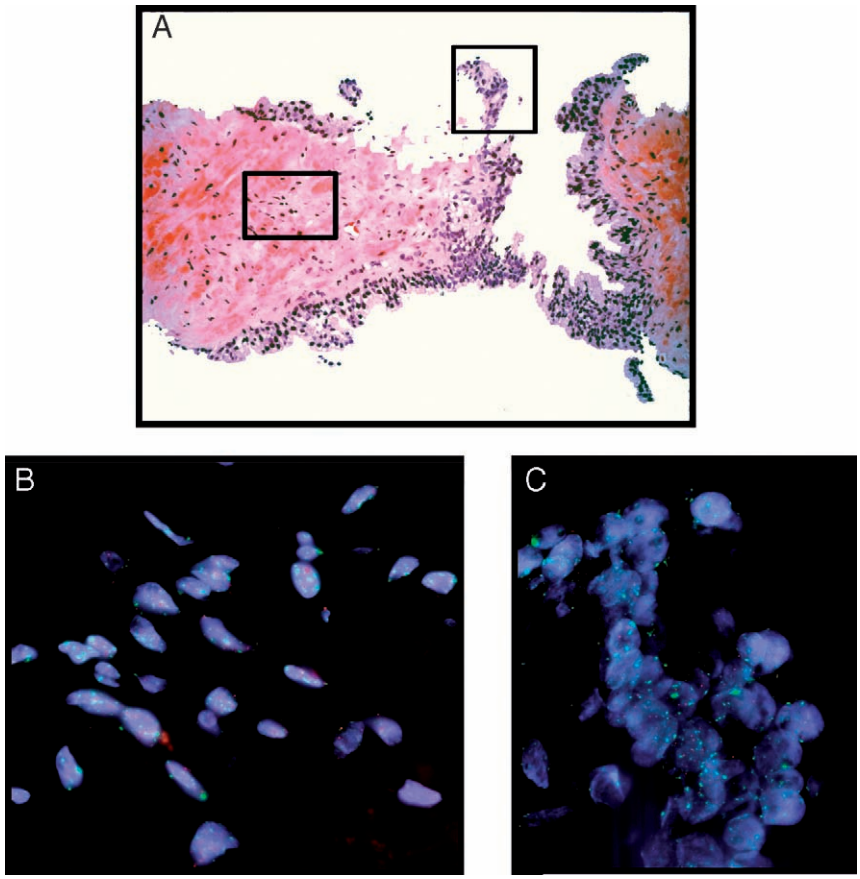

Figure 1. *A representative example of the analysis used in HPIN biopsies. (A) Areas of interest were identified and corresponding QFISH images were generated on a deeper slice of the tissue, with corresponding areas of stroma (B) and HPIN (C) analyzed. The images have been colored to facilitate visual inspection with telomere PNA probe (Cy3—red) and centromere PNA probe (FITC—green).*

(HPIN + PSA: $P = .006$; stroma + PSA: $P = .010$; PSA + HPIN + stroma: $P = .015$).

Site of cancer and Gleason score There did not appear to be any relationship between the telomere length of biopsy and the ultimate Gleason score of prostate tumors (Figure 4*B*). To determine whether the relative telomere length within different regions of the gland at the time of biopsy was predictive of the site that was subsequently diagnosed with cancer, a comparison between the actual sites biopsied and the side of the gland that was diagnosed with cancer was performed (Figure 4*C*). Although the numbers are limited, trends in both HPIN and stromal telomere length suggest that attrition in biopsy sites that eventually had cancer detected were indeed shorter than the attrition in biopsy sites where cancer was detected on the same side but at a different site or on the opposite side of the gland.

Analyses from Stratification of Telomere Length

As a further exploratory analysis, telomere length was stratified into ''short'' and ''long'' based on the statistical standard of median values. Kaplan-Meier analysis of the time to diagnosis of cancer stratified by telomere length in HPIN reveals a trend to significance ($P = .126$; HR = 1.72; 95% CI = 0.287–1.168); however, a similar analysis of telomere length in stroma reveals a significant finding ($P = .0346$; HR = 2.12; 95% CI = 0.231–0.956) (Figure 3, *C* and *D*). A trend was also noted for PSA ($P = .093$; HR = 1.8; 95% CI = 0.892–3.632), but not for age ($P = .522$; HR = 0.8; 95% CI = 0.632–2.570).

Discussion

Understanding the molecular processes driving prostatic carcinogenesis has important clinical consequences, as HPIN biopsy and autopsy studies [30] suggest that PIN may precede cancer by about a decade. Previously, our laboratory demonstrated a decline in telomere length in radical prostatectomy samples in the progression from benign epithelium to HPIN far from the cancer, to HPIN close to the cancer, to CaP itself [8]. The present QFISH study appears to be the first to examine normalized telomere length measurements using cell-by-cell analyses of both preneoplastic epithelial tissues and stromal components of the prostate in a large-enough cohort to detect a correlation between epithelial and stromal telomere lengths (Figure 1).

The detailed results presented herein reveal interesting insights concerning both telomere biology and the process of prostatic preneoplasia. The 22% increase in centromeric material in HPIN compared to that in the stroma (Figure 2*A*)

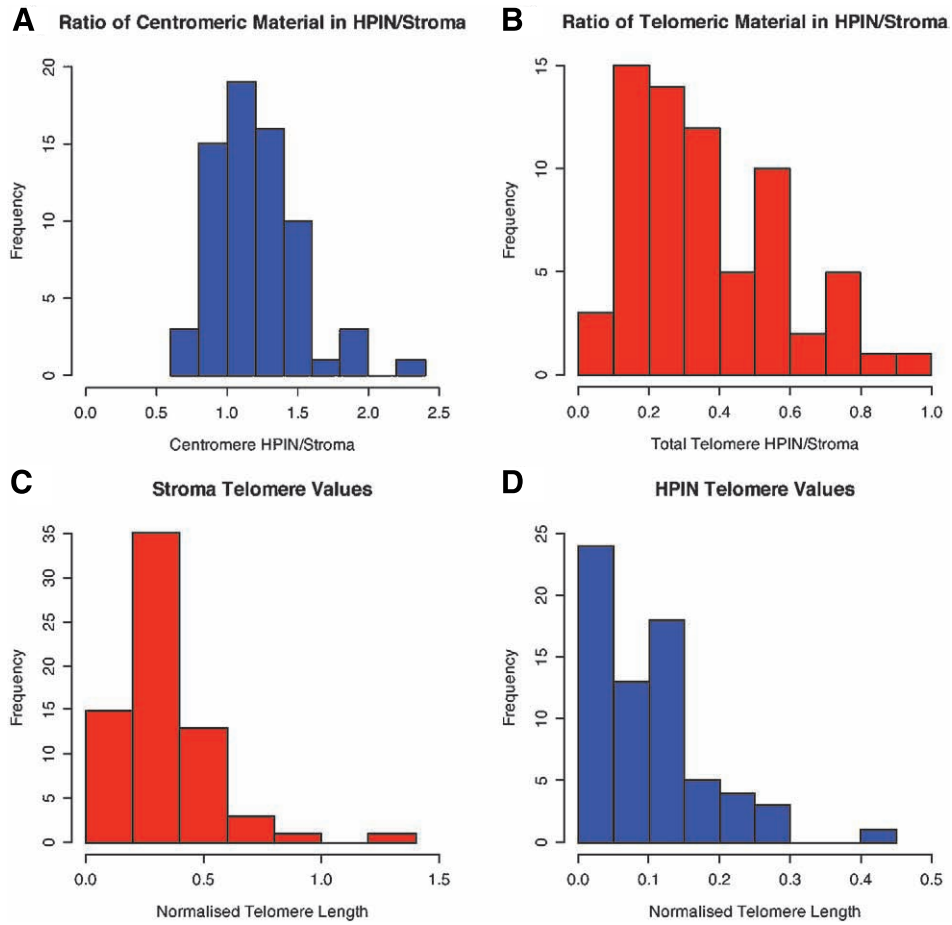

Figure 2. *To examine the relative amount of chromosomal material in the HPIN versus the amount of chromosomal material in the surrounding stroma, we plotted (A) the frequency distribution of the ratio of centromeric fluorescence intensity measurements in HPIN compared to that in the surrounding stroma. An average increase of 22% (SD 31%) was found in HPIN compared to that found in the surrounding stroma. To examine the relative amount of telomere attrition in the prostate, we plotted (B) the frequency distribution of the ratio of the telomeric fluorescence in HPIN divided by that in the surrounding stroma. As mentioned in the text, an average 64% decrease of the surrounding stroma (SD = 21%) was found. (C) Frequency distribution of normalized telomere values (telomeric fluorescence/centromeric fluorescence) in the HPIN and (D) in the stroma of the study cohort.*

is consistent with previous studies from our laboratory, indicating that, in early HPIN, gross ploidy change is rare, although subsets of patients have characteristic chromosomal gains [7]. The 64% reduction in telomere length in the same tissue (Figure 2*B*) may simply be a surrogate marker for the number of times that the preneoplastic epithelium, compared to the surrounding stroma, has replicated. However, a number of factors may also influence telomere length because ploidy change, concurrent telomerase expression [19,20], and additive oxidative stress [31] are all likely to influence the relative rates of attrition. Importantly, the findings of the present study are coherent with that of Meeker et al., who examined 11 HPIN lesions from six patients after radical prostatectomy. Similar telomeric fluorescence in prostatic stromal and basal epithelial cells was found, with a 3.7-fold (or 73%) decrease in luminal HPIN compared to that in basal cells—comparable to our finding of a 2.8-fold (or 64%) decrease compared to that in the surrounding stroma.

Overall, the data suggest that those men with biopsies with shorter telomeres have features that either directly or indirectly lead to a greater likelihood of a diagnosis of cancer. Shorter telomeres may either have been inherited as a constitutional trait or have been acquired somatically because of attrition induction by tissue-specific environmental factors. In either case, in HPIN lesions bearing longer telomeres, they may have been acting initially as a tumor-suppressor mechanism, as prostatic epithelial cells do not possess enough permissive mutations for continued proliferation to take place in the setting of a telomere-induced DNA damage signal [10]. Current models suggest that if

Table 2. *P* Values Associated with the Prediction of CaP from Telomere Length Analysis.

Time	Men at Risk (*n*)	HPIN	Stroma	PSA	HPIN + PSA	Stroma + PSA
Immediately	68	.026	.029	.021	.012	.010
3 months	64	.050	.038	.032	.019	.015
6 months	61	.075	.046	.046	.036	.026
12 months	56	.056	.043	.107	.049	.046

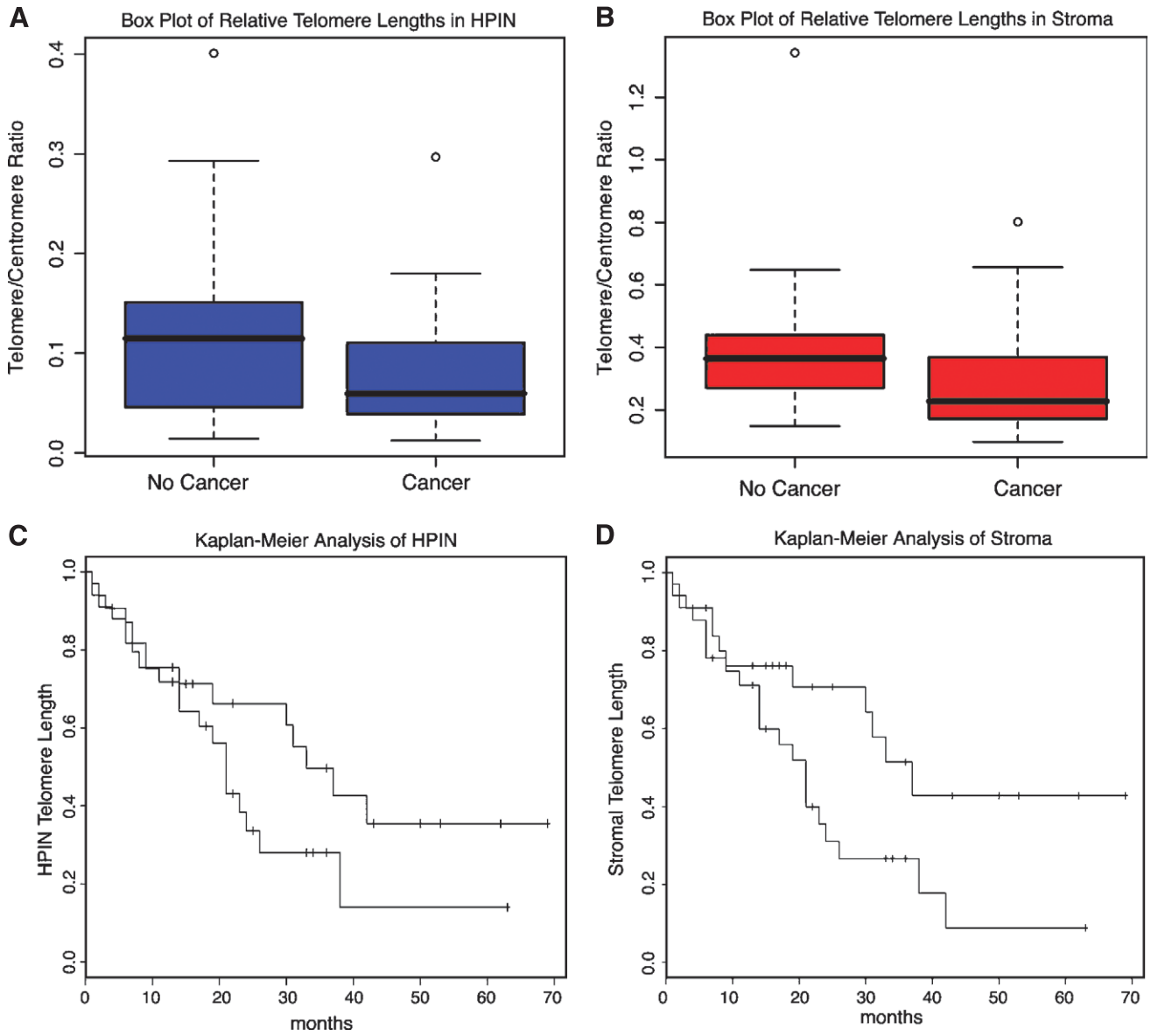

Figure 3. *(A) Boxplot of relative telomere length in HPIN comparing groups of men who developed cancer and men who did not develop cancer. The thick black line represents median values. The upper border of the blue rectangle represents the 25th percentile, and the lower border represents the 75th percentile. Circles represent outliers based on × 1.5 interquartile range. Bars extending above and below represent the upper and lower limits of data (t-test: P = .03; 95% CI = 0.004–0.080). (B) Boxplot of relative telomere length in the stroma comparing groups of men who developed cancer and men who did not develop cancer. Boxplot variables and numbers are similar to (A) (t-test: P = .04; 95% CI = 0.004–0.188). (C) Kaplan-Meier analysis of HPIN telomere length, stratified by the median value for the time to develop cancer (P = .126; HR = 1.72; 95% CI = 0.287–1.168). (D) Kaplan-Meier analysis of stromal telomere length, stratified by the median value for the time to develop cancer (P = .0346; HR = 2.12; 95% CI = 0.231–0.956).*

continued proliferation occurs, telomere length may simply be acting as a mitotic clock. It follows that areas of HPIN with shorter telomeres will have replicated more and will have had a greater opportunity to accumulate stochastic events that ultimately lead to genomic instability and acquisition of chromosomal rearrangements associated with the emergence of carcinoma [8].

Alternatives to this model involve an appreciation of cellular senescence phenomena. Senescence in the setting of preneoplasia is thought to occur due to either telomere attrition eliciting a DNA damage response or inappropriate oncogene activation, likely through p16 [32]. Thus, certain HPIN lesions (presumably those with longer telomeres) may be arrested due to oncogene-induced senescence—a phenomenon that has received a great deal of interest recently [33]. Those HPIN cells with relatively short telomeres will presumably lack the molecular machinery to elicit an oncogene-induced senescence response. Eventually, telomere-generated chromosomal instability is likely to occur, leading to the onset of neoplasia. Senescence phenomena are currently relatively poorly understood in prostatic carcinogenesis [34]. Two recent papers have provided support for the role of oncogene-induced senescence in this context. Fan et al. [35] demonstrated high levels of

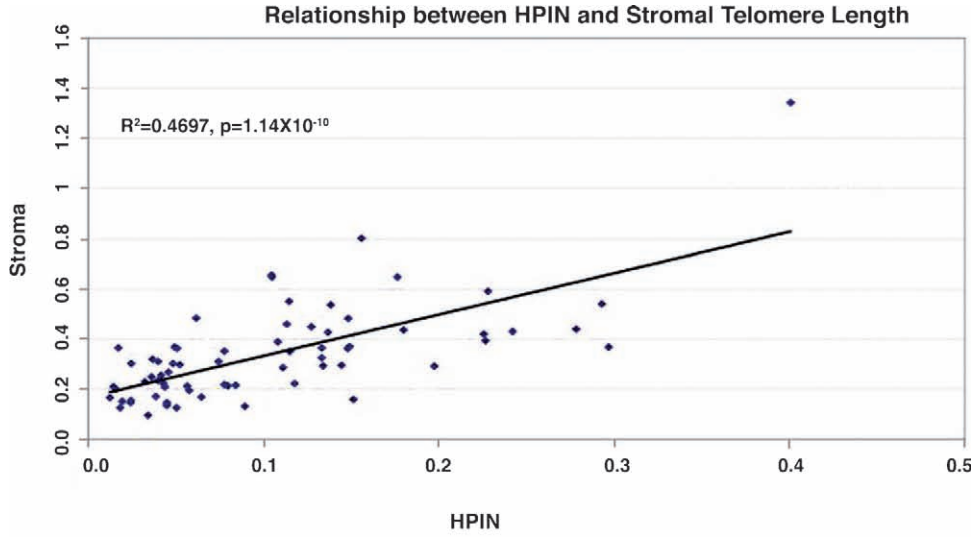

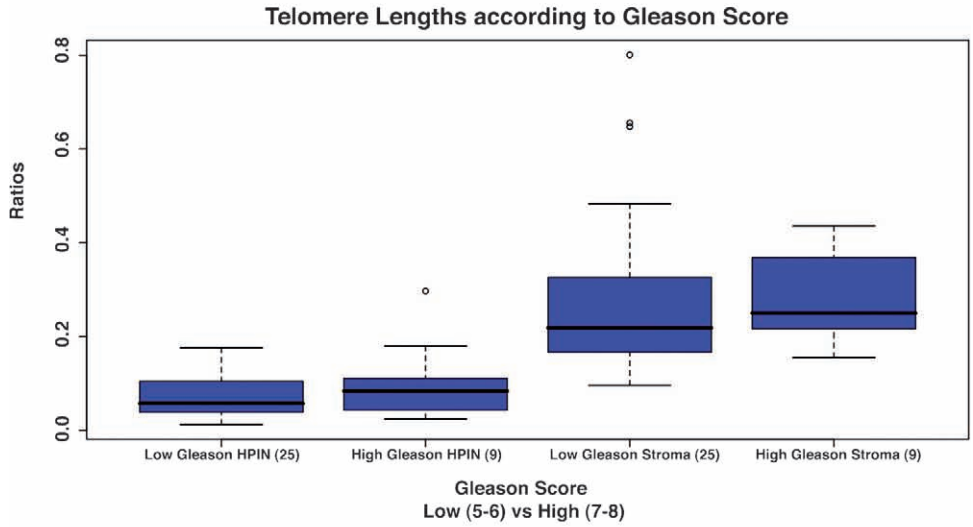

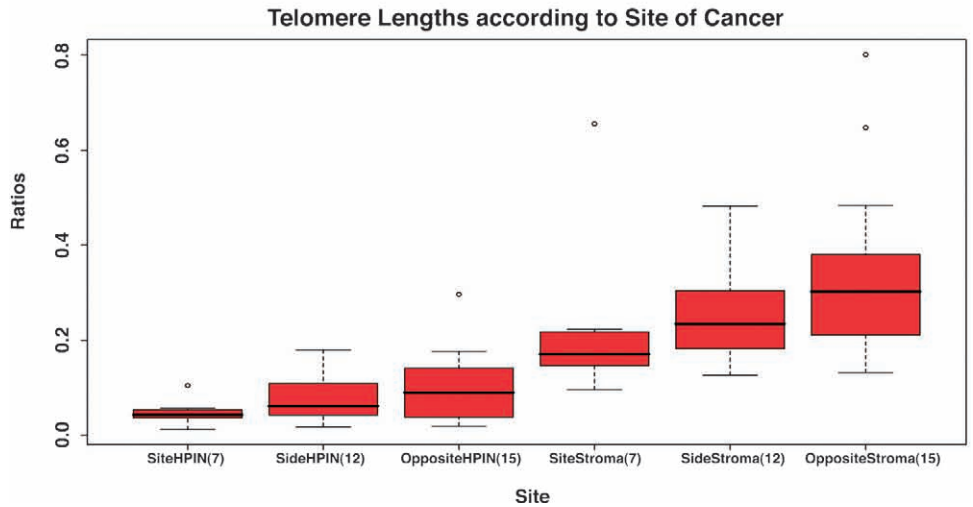

Figure 4. *(A) Relationship between normalized HPIN and stromal telomere length in prostatic biopsies examined. Normalized telomere length reflects telomere intensities controlled for centromeric intensities. R^2 values are indicated. (B) Boxplots of normalized telomere lengths in HPIN and in the stroma, according to the Gleason score of eventual cancer. Because of limited numbers, cases were grouped according to low (5–6) and high Gleason scores (6–7). Numbers in brackets adjacent to labels on the x-axis represent the number of cases with that outcome in the cohort. Boxplot variables and numbers are similar to those in Figure 3 A. (C) Boxplots represent sites of diagnosis of CaP grouped by their relationship to where the biopsy was analyzed. Boxplot variables and numbers are similar to those in Figure 3 A. X-axis labels refer to the type of analysis: either HPIN or surrounding stroma, with the preceding letters referring to the site of the eventual cancer; either the same site, the same side, or the opposite side of the prostate gland. Numbers in brackets refer to the number of men in those groups.*

activated ATM and other proteins involved in DNA damage response in HPIN, whereas a *PTEN* knockout model of CaP found heterozygous *PTEN* deletion leading to a p53-dependent senescence barrier that would likely be premature for a telomere-induced barrier and also limited staining of human HPIN lesions with β-galactosidase, a traditional marker of senescent cells [36].

Current evidence suggests that histologically normal prostatic tissues adjacent to a CaP may harbor subtle oncogenic changes [37–39]; however, there are only limited data suggesting that the surrounding stroma is also subject to oncogenic modification [40]. Preliminary evidence of such a phenomenon was first reported by Fordyce et al. [37] who found reduced telomere length in histologically normal prostate tissues (containing both the epithelium and the stroma) in tissues adjacent to the foci of CaP. The finding presented in the present study, indicating that telomere attrition is partly attributable to the stroma alone, has important implications. Firstly, as the prostatic stroma is not thought to replicate to any significant degree during the process of prostatic carcinogenesis, these data suggest that etiologic factors postulated to be related to prostatic carcinogenesis may affect both compartments of the prostatic microarchitecture. Dietary antioxidant deficiency and chronic inflammation are considered candidates for this effect, as they both act through oxidative stress, to which telomeres are known to be particularly susceptible [41,42]. Secondly, corroborative evidence [43] suggests that senescent prostatic fibroblasts (which are likely to be those with short telomeres) secrete a number of growth factors, such as hepatocyte growth factor (HGF), that may facilitate prostatic carcinogenesis through mechanisms such as coactivation of androgen receptor signaling [44]. Taken together, these studies suggest a link between the well-established role of tumor–stromal interaction [45] and telomere dysfunction in prostatic carcinogenesis.

Despite the intriguing observations made, there are limitations to this analysis. The patient biopsies originated from different community practices throughout Ontario, Canada, and did not have consistent time-mandated or event-mandated biopsies. We were limited in only analyzing one HPIN-containing biopsy site in the sextant biopsy set from every man, rather than a more thorough analysis of telomere length in every biopsy site, which would allow a greater understanding of the evolution of telomere dysfunction in the three-dimensional anatomy of the prostate gland. Additionally, ascertaining telomerase expression would have been useful in our cohort; however, there are currently no reliable methodologies to do this in paraffin-embedded sections [46]. Unfortunately, normal peripheral blood was not available to further explore the contribution of constitutional telomere length in this study. Finally, it is possible that a proportion of the men who were diagnosed with CaP during the study period had foci of neoplasia that were missed on initial biopsy.

In conclusion, there are a number of emerging markers of CaP in progress [47,48]. This study suggests that telomere attrition analysis may assist with diagnosis and prognosis in prostatic neoplasia.

Acknowledgements

We thank Salomon Minkin, Lea Harrington, and Ian Tannock for their helpful suggestions and review.

References

[1] The American Cancer Society (2006). Cancer Facts and Figures, 2006 (Available from http://www.cancer.org/downloads/STT/CAFF2006PWSecured.pdf (cited May 23, 2006)).

[2] Canadian Cancer Society and National Cancer Institute of Canada (2006). Canadian Cancer Statistics 2006 (Available from http://129.33.170.32/vgn/images/portal/cit_86751114/31/21/935505792cw_2006stats_en.pdf.pdf (cited May 23, 2006)).

[3] Qian J, Wollan P, and Bostwick DG (1997). The extent and multicentricity of high-grade prostatic intraepithelial neoplasia in clinically localized prostatic adenocarcinoma. *Hum Pathol* **28** (2), 143–148.

[4] Sakr WA, Grignon DJ, Crissman JD, Heilbrun LK, Cassin BJ, Pontes JJ, and Haas GP (1994). High grade prostatic intraepithelial neoplasia (HGPIN) and prostatic adenocarcinoma between the ages of 20–69: an autopsy study of 249 cases. *In Vivo* **8** (3), 439–443.

[5] Sakr WA, Haas GP, Cassin BF, Pontes JE, and Crissman JD (1993). The frequency of carcinoma and intraepithelial neoplasia of the prostate in young male patients. *J Urol* **150** (2 (Pt 1)), 379–385.

[6] Beheshti B, Vukovic B, Marrano P, Squire JA, and Park PC (2002). Resolution of genotypic heterogeneity in prostate tumors using polymerase chain reaction and comparative genomic hybridization on microdissected carcinoma and prostatic intraepithelial neoplasia foci. *Cancer Genet Cytogenet* **137** (1), 15–22.

[7] Al-Maghrabi J, Vorobyova L, Toi A, Chapman W, Zielenska M, and Squire JA (2002). Identification of numerical chromosomal changes detected by interphase fluorescence *in situ* hybridization in high-grade prostate intraepithelial neoplasia as a predictor of carcinoma. *Arch Pathol Lab Med* **126** (2), 165–169.

[8] Vukovic B, Park PC, Al-Maghrabi J, Beheshti B, Sweet J, Evans A, Trachtenberg J, and Squire J (2003). Evidence of multifocality of telomere erosion in high-grade prostatic intraepithelial neoplasia (HPIN) and concurrent carcinoma. *Oncogene* **22** (13), 1978–1987.

[9] Meeker AK, Hicks JL, Platz EA, March GE, Bennett CJ, Delannoy MJ, and De Marzo AM (2002). Telomere shortening is an early somatic DNA alteration in human prostate tumorigenesis. *Cancer Res* **62** (22), 6405–6409.

[10] Meeker AK (2006). Telomeres and telomerase in prostatic intraepithelial neoplasia and prostate cancer biology. *Urol Oncol* **24** (2), 122–130.

[11] Cerveira N, Ribeiro FR, Peixoto A, Costa V, Henrique R, Jeronimo C, and Teixeira MR (2006). *TMPRSS2–ERG* gene fusion causing ERG overexpression precedes chromosome copy number changes in prostate carcinomas and paired HGPIN lesions. *Neoplasia* **8** (10), 826–832.

[12] Yoshimoto M, Cutz JC, Nuin PAS, Joshua AM, Bayani J, Evans AJ, Zielenska M, and Squire JA (2006). Interphase FISH analysis of PTEN in histological sections shows genomic deletions in 68% of primary prostate cancer and 23% of high-grade prostatic intra-epithelial neoplasias. *Cancer Genet Cytogenet* **169** (2), 128–137.

[13] Moyzis RK, Buckingham JM, Cram LS, Dani M, Deaven LL, Jones MD, Meyne J, Ratliff RL, and Wu JR (1988). A highly conserved repetitive DNA sequence, $(TTAGGG)_n$, present at the telomeres of human chromosomes. *Proc Natl Acad Sci USA* **85** (18), 6622–6626.

[14] Maser RS and DePinho RA (2004). Telomeres and the DNA damage response: why the fox is guarding the henhouse. *DNA Repair (Amsterdam)* **3** (8–9), 979–988.

[15] Ohki R, Tsurimoto T, and Ishikawa F (2001). *In vitro* reconstitution of the end replication problem. *Mol Cell Biol* **21** (17), 5753–5766.

[16] Mathieu N, Pirzio L, Freulet-Marriere MA, Desmaze C, and Sabatier L (2004). Telomeres and chromosomal instability. *Cell Mol Life Sci* **61** (6), 641–656.

[17] Artandi SE and DePinho RA (2000). A critical role for telomeres in suppressing and facilitating carcinogenesis. *Curr Opin Genet Dev* **10** (1), 39–46.

[18] Bettendorf O, Heine B, Kneif S, Eltze E, Semjonow A, Herbst H, Stein H, Bocker W, and Poremba C (2003). Expression-patterns of the RNA component (hTR) and the catalytic subunit (hTERT) of human telomerase in nonneoplastic prostate tissue, prostatic intraepithelial neoplasia, and prostate cancer. *Prostate* **55** (2), 99–104.

[19] Koeneman KS, Pan CX, Jin JK, Pyle JM III, Flanigan RC, Shankey TV, and Diaz MO (1998). Telomerase activity, telomere length, and

DNA ploidy in prostatic intraepithelial neoplasia (PIN). *J Urol* **160** (4), 1533–1539.

[20] Zhang W, Kapusta LR, Slingerland JM, and Klotz LH (1998). Telomerase activity in prostate cancer, prostatic intraepithelial neoplasia, and benign prostatic epithelium. *Cancer Res* **58** (4), 619–621.

[21] Tomlins SA, Rhodes DR, Perner S, Dhanasekaran SM, Mehra R, Sun XW, Varambally S, Cao X, Tchinda J, Kuefer R, et al. (2005). Recurrent fusion of *TMPRSS2* and *ETS* transcription factor genes in prostate cancer. *Science* **310** (5748), 644–648.

[22] Yoshimoto M, Joshua AM, Chilton-MacNeill S, Bayani J, Selvarajah S, Evans AJ, Zielenska M, and Squire JA (2006). Three-color FISH analysis of TMPRSS2/ERG fusions in prostate cancer indicates that genomic microdeletion of chromosome 21 is associated with rearrangement. *Neoplasia* **8** (6), 465–469.

[23] Bostwick DG, Shan A, Qian J, Darson M, Maihle NJ, Jenkins RB, and Cheng L (1998). Independent origin of multiple foci of prostatic intraepithelial neoplasia: comparison with matched foci of prostate carcinoma. *Cancer* **83** (9), 1995–2002.

[24] Wu X, Amos CI, Zhu Y, Zhao H, Grossman BH, Shay JW, Luo S, Hong WK, and Spitz MR (2003). Telomere dysfunction: a potential cancer predisposition factor. *J Natl Cancer Inst* **95** (16), 1211–1218.

[25] Tabori U, Vukovic B, Zielenska M, Hawkins C, Braude I, Rutka J, Bouffet E, Squire J, and Malkin D (2006). The role of telomere maintenance in the spontaneous growth arrest of pediatric low-grade gliomas. *Neoplasia* **8** (2), 136–142.

[26] Poon SS, Martens UM, Ward RK, and Lansdorp PM (1999). Telomere length measurements using digital fluorescence microscopy. *Cytometry* **36** (4), 267–278.

[27] Abramoff MD, Magelhaes PJ, and Ram SJ (2004). Image processing with Image J. *Biophoton Int* **11** (7), 36–42.

[28] Meeker AK (2003). Improved software for quantitative analysis of fluorescence microscopy images. *Advancing Practice, Instruction and Innovation through Informatics*.

[29] Team RDC (2006). R: A Language and Environment for Statistical Computing R Foundation for Statistical Computing, Vienna, Austria.

[30] Bostwick DG and Qian J (2004). High-grade prostatic intraepithelial neoplasia. *Mod Pathol* **17** (3), 360–379.

[31] von Zglinicki T (2002). Oxidative stress shortens telomeres. *Trends Biochem Sci* **27** (7), 339–344.

[32] Sherr CJ, Bertwistle D, Besten WDEN, Kuo ML, Sugimoto M, Tago K, Williams RT, Zindy F, and Roussel MF (2005). p53-Dependent and -independent functions of the Arf tumor suppressor. *Cold Spring Harb Symp Quant Biol* **70,** 129–137.

[33] Christophorou MA, Ringshausen I, Finch AJ, Swigart LB, and Evan GI (2006). The pathological response to DNA damage does not contribute to p53-mediated tumour suppression. *Nature* **443** (7108), 214–217.

[34] Schwarze SR, Fu VX, Desotelle JA, Kenowski ML, and Jarrard DF (2005). The identification of senescence-specific genes during the induction of senescence in prostate cancer cells. *Neoplasia* **7** (9), 816–823.

[35] Fan C, Quan R, Feng X, Gillis A, He L, Matsumoto ED, Salama S, Cutz JC, Kapoor A, and Tang D (2006). ATM activation is accompanied with earlier stages of prostate tumorigenesis. *Biochim Biophys Acta* **1763** (10), 1090–1097.

[36] Chen Z, Trotman LC, Shaffer D, Lin HK, Dotan ZA, Niki M, Koutcher JA, Scher HI, Ludwig T, Gerald W, et al. (2005). Crucial role of p53-dependent cellular senescence in suppression of Pten-deficient tumorigenesis. *Nature* **436** (7051), 725–730.

[37] Fordyce CA, Heaphy CM, Joste NE, Smith AY, Hunt WC, and Griffith JK (2005). Association between cancer-free survival and telomere DNA content in prostate tumors. *J Urol* **173** (2), 610–614.

[38] Donaldson L, Fordyce C, Gilliland F, Smith A, Feddersen R, Joste N, Moyzis R, and Griffith J (1999). Association between outcome and telomere DNA content in prostate cancer. *J Urol* **162** (5), 1788–1792.

[39] Merseburger AS, Hennenlotter J, Simon P, Muller CC, Kuhs U, Knuchel-Clarke R, Moul JW, Stenzl A, and Kuczyk MA (2006). Activation of the PKB/Akt pathway in histological benign prostatic tissue adjacent to the primary malignant lesions. *Oncol Rep* **16** (1), 79–83.

[40] Hanson JA, Gillespie JW, Grover A, Tangrea MA, Chuaqui RF, Emmert-Buck MR, Tangrea JA, Libutti SK, Linehan WM, and Woodson KG (2006). Gene promoter methylation in prostate tumor-associated stromal cells. *J Natl Cancer Inst* **98** (4), 255–261.

[41] Oikawa S, Tada-Oikawa S, and Kawanishi S (2001). Site-specific DNA damage at the GGG sequence by UVA involves acceleration of telomere shortening. *Biochemistry* **40** (15), 4763–4768.

[42] Kawanishi S and Oikawa S (2004). Mechanism of telomere shortening by oxidative stress. *Ann NY Acad Sci* **1019,** 278–284.

[43] Bavik C, Coleman I, Dean JP, Knudsen B, Plymate S, and Nelson PS (2006). The gene expression program of prostate fibroblast senescence modulates neoplastic epithelial cell proliferation through paracrine mechanisms. *Cancer Res* **66** (2), 794–802.

[44] Nakashiro K, Okamoto M, Hayashi Y, and Oyasu R (2000). Hepatocyte growth factor secreted by prostate-derived stromal cells stimulates growth of androgen-independent human prostatic carcinoma cells. *Am J Pathol* **157** (3), 795–803.

[45] Olumi AF, Grossfeld GD, Hayward SW, Carroll PR, Tlsty TD, and Cunha GR (1999). Carcinoma-associated fibroblasts direct tumor progression of initiated human prostatic epithelium. *Cancer Res* **59** (19), 5002–5011.

[46] Wu YL, Dudognon C, Nguyen E, Hillion J, Pendino F, Tarkanyi I, Aradi J, Lanotte M, Tong JH, Chen GQ, et al. (2006). Immunodetection of human telomerase reverse-transcriptase (hTERT) re-appraised: nucleolin and telomerase cross paths. *J Cell Sci* **119** (Pt 13), 2797–2806.

[47] Laxman B, Tomlins SA, Mehra R, Morris DS, Wang L, Helgeson BE, Shah RB, Rubin MA, Wei JT, and Chinnaiyan AM (2006). Noninvasive detection of TMPRSS2:ERG fusion transcripts in the urine of men with prostate cancer. *Neoplasia* **8** (10), 885–888.

[48] Paul B, Dhir R, Landsittel D, Hitchens MR, and Getzenberg RH (2005). Detection of prostate cancer with a blood-based assay for early prostate cancer antigen. *Cancer Res* **65** (10), 4097–4100.